© 2022. Published by The Company of Biologists Ltd | Development (2022) 149, dev199575. doi:10.1242/dev.199575

RESEARCH ARTICLE

Embryonic requirements for *Tcf12* in the development of the mouse coronal suture

Man-chun Ting[1], D'Juan T. Farmer[2], Camilla S. Teng[1,2], Jinzhi He[3], Yang Chai[3], J. Gage Crump[2,*] and Robert E. Maxson[1,2,*]

ABSTRACT

A major feature of Saethre-Chotzen syndrome is coronal craniosynostosis, the fusion of the frontal and parietal bones at the coronal suture. It is caused by heterozygous loss-of-function mutations in either of the bHLH transcription factors *TWIST1* and *TCF12*. Although compound heterozygous *Tcf12*; *Twist1* mice display severe coronal synostosis, the individual role of *Tcf12* had remained unexplored. Here, we show that Tcf12 controls several key processes in calvarial development, including the rate of frontal and parietal bone growth, and the boundary between sutural and osteogenic cells. Genetic analysis supports an embryonic requirement for *Tcf12* in suture formation, as combined deletion of *Tcf12* in embryonic neural crest and mesoderm, but not in postnatal suture mesenchyme, disrupts the coronal suture. We also detected asymmetric distribution of mesenchymal cells on opposing sides of the wild-type frontal and parietal bones, which prefigures later bone overlap at the sutures. In *Tcf12* mutants, reduced asymmetry is associated with bones meeting end-on-end, possibly contributing to synostosis. Our results support embryonic requirements of Tcf12 in proper formation of the overlapping coronal suture.

KEY WORDS: Cranial suture, Craniosynostosis, *Tcf12*, *Twist1*, Osteogenic stem cells, Mouse

INTRODUCTION

Craniosynostosis, the pathological fusion of the flat bones forming the top of the skull, occurs in ∼1/2000 live births (Lajeunie et al., 1995). Fusion occurs at fibrous joints called sutures that allow the skull to flex during childbirth and mastication. Craniosynostosis occurs in both sporadic and syndromic forms, and often affects particular sutures (Wilkie et al., 2006; Johnson and Wilkie, 2011). The coronal suture forms between the frontal and parietal bones and is preferentially affected in Saethre-Chotzen syndrome. The molecular genetics of this disorder have been under investigation for over two decades (Wilkie, 1997; Jabs, 2008). It is inherited as an autosomal dominant and has an incidence of 1/50,000 live births. In addition to coronal craniosynostosis, affected individuals also exhibit, with varying penetrance, digital abnormalities, abnormal facial structure and intellectual disability (Twigg and Wilkie, 2015). Heterozygous loss-of-function mutations in either of the basic helix-loop-helix (bHLH) transcription factor genes *TWIST1* and *TCF12* account for most Saethre-Chotzen syndrome cases (Howard et al., 1997; El Ghouzzi et al., 1997; Sharma et al., 2013). Twist1 belongs to a subfamily of bHLH proteins, members of which are expressed in specific tissues or cell types (Massari and Murre, 2000; Wang and Baker, 2015). Tcf12 is a member of the E protein subfamily of bHLH proteins, members of which typically exhibit broad expression (Wang and Baker, 2015). In mice, heterozygous deletion of *Twist1* phenocopies the selective coronal suture loss seen in human Saethre-Chotzen patients (El Ghouzzi et al., 1997). Whereas heterozygosity of *Tcf12* alone does not result in suture defects in mice, it does enhance coronal synostosis in *Twist1*+/– mice (Sharma et al., 2013). In zebrafish, loss of *tcf12* or *twist1b* alone does not cause craniosynostosis, yet combined homozygous loss of *twist1b* and *tcf12* results in coronal-specific synostosis (Teng et al., 2018), despite the zebrafish coronal suture likely not being homologous with the murine coronal suture (Teng et al., 2019). Although these experiments show combined requirements of Twist1 and Tcf12 for early development of the coronal suture (Teng et al., 2018), the individual role of Tcf12 in skull development had remained unexplored in model organisms, leaving it unclear whether Twist1 and Tcf12 control similar or distinct processes during suture development.

In mice and zebrafish, combinatorial loss of *Twist1* and *Tcf12* alleles influences the dynamics of osteogenic precursors during embryonic calvarial bone development (Teng et al., 2018). In compound mutants, frontal and parietal bone growth was accelerated, with the degree of acceleration in zebrafish predictive of later coronal suture loss. In addition to effects on osteogenic precursor dynamics in compound *Twist1; Tcf12* heterozygous mice, heterozygous loss of *Twist1* also results in inappropriate cell mixing at the boundary between the neural crest-derived frontal and mesoderm-derived parietal bones (Merrill et al., 2006; Ting et al., 2009). Loss-of-function of the ephrin receptor, EphA4, also causes cell mixing at the neural crest-mesoderm boundary and results in synostosis of the frontal and parietal bones (Merrill et al., 2006). *Twist1* function is required in both neural crest-derived and mesoderm-derived cells for suture formation, with only heterozygous loss of *Twist1* in both tissues resulting in synostosis (Teng et al., 2018). However, as these studies used non-conditional Cre drivers, distinct requirements in embryonic versus postnatal sutures could not be distinguished. This is a significant caveat, as recent work has demonstrated that the postnatal suture is a continuous source of osteogenic cells for the growth and repair of the calvarial bones. For example, *Gli1:CreER* can be used to mark long-term stem cells in the postnatal mouse suture, with genetic ablation of these labeled cells resulting in loss of all sutures (Zhao et al., 2015).

[1]Department of Biochemistry and Molecular Medicine, Keck School of Medicine, University of Southern California, Los Angeles, CA 90033, USA. [2]Department of Stem Cell Biology and Regenerative Medicine, University of Southern California, Los Angeles, CA 90033, USA. [3]Center for Craniofacial Molecular Biology, School of Dentistry, University of Southern California, Los Angeles, CA 90033, USA.

*Authors for correspondence (maxson@usc.edu, gcrump@usc.edu)

M.T., 0000-0002-5609-5032; C.S.T., 0000-0002-8150-3050; Y.C., 0000-0003-2477-7247; J.G.C., 0000-0002-3209-0026; R.E.M., 0000-0002-9141-9389

Handling Editor: Patrick Tam
Received 2 March 2021; Accepted 22 November 2021

Development (2022) 149, dev199575. doi:10.1242/dev.199575

Twist1 can form homodimers as well as heterodimers with a variety of bHLH factors, including Tcf12 (Fan et al., 2020). Forced dimer approaches in embryonic stem cells (Fan et al., 2020) and in mouse sutures (Connerney et al., 2006) have provided evidence that Twist1 homodimers and Twist1-E heterodimers drive different cellular processes. In differentiating mouse embryonic stem cells, heterodimers promote expression of ectodermal and mesodermal markers and homodimers maintain cells in a pluripotent state. In developing mouse sutures, a higher Twist1/Twist1 to Twist1/E ratio was associated with an expansion of the osteogenic fronts and suture closure (Connerney et al., 2006). It thus appears to be clear that a change in the ratio of Twist1 homodimers versus Twist1-E heterodimers can produce different biological outcomes, although the exact role of Twist1 homodimers and heterodimers in suture development and craniosynostosis remains unclear.

Here, we investigate the extent to which Tcf12, a binding partner for Twist1 (Fan et al., 2020), participates in developmental processes of suture formation similar to those described for Twist1. In contrast to the expectation from forced dimer approaches, we show that homozygous loss of *Tcf12* recapitulates many of the calvarial phenotypes of heterozygous *Twist1* and compound heterozygous *Twist1; Tcf12* mice, including accelerated frontal and parietal bone growth, and disruption of the boundary between sutural and osteogenic cells. We also find that Tcf12 function is required in both neural crest-derived and mesoderm-derived cells for coronal suture formation. The suture mesenchyme between the apposing frontal and parietal bones has been shown to house skeletal stem cells (Zhao et al., 2015). In the appendicular skeleton, Grem1 marks mesenchymal progenitors responsible for bone formation (Worthley et al., 2015). Interestingly, we find that Tcf12 also controls the asymmetry of Grem1+ mesenchyme cells at the parietal and frontal bone fronts, which may help explain the predictable overlapping nature of these bones at the normal coronal suture. In addition, we show that conditional deletion of *Tcf12* in the postnatal *Gli1*+ sutural stem cell domain does not affect maintenance of sutures, further pointing to a largely embryonic role of Tcf12 in suture regulation.

RESULTS

Homozygous loss of *Tcf12* disrupts coronal suture formation

To investigate the role of the murine *Tcf12* gene in the development of craniosynostosis, we generated a *Tcf12* null allele by crossing $Tcf12^{flox/flox}$ mice with EIIa-Cre, a general deleter active in the germline (Lakso et al., 1996). It had previously been reported that homozygous $Tcf12^{-/-}$ mice are born at the expected frequency from a $Tcf12^{+/-}$ incross, with the vast majority dying by 2 weeks after birth (Zhuang et al., 1996). We similarly observed that most homozygous $Tcf12^{-/-}$ mice died within the first 2 weeks. In order to examine the morphology of the coronal suture, we carried out Alizarin Red staining on the skulls from homozygous *Tcf12* mutants. We found partial fusion of the coronal suture in 5 of 10 $Tcf12^{-/-}$ mice (50%) at embryonic stages [embryonic day (E)17-E18] and 8 of 22 $Tcf12^{-/-}$ mice (36%) surviving into postnatal stages [postnatal day (P)0-P21]; no coronal suture defects were observed in 35 heterozygous $Tcf12^{+/-}$ and 26 wild-type sibling mice (Fig. 1; Movies 1, 2; Table 1,). The mutant parietal bones displayed an abnormal overlap at the sagittal suture at E18, P0 and P2 stages. We also observed developmental delay and rare exencephaly in $Tcf12^{-/-}$ mice, as reported by Zhuang, et al. (1996), with the frequency of exencephaly increasing from 3% to 33% when one allele of *Twist1* was also deleted (Table 2). In addition, $Tcf12^{-/-}$ mice displayed kinks and curls of the tail, a phenotype known to be caused by a moderate delay in posterior neuropore closure (van Straaten and Copp, 2001). $Tcf12^{-/-}$; $Twist1^{+/-}$ mice also infrequently displayed an open ventral body wall not observed in $Tcf12^{-/-}$ mice (Table 2). The suture phenotypes and low-penetrance exencephaly and associated defects suggest that *Tcf12* functions in both calvarial suture development and neurulation.

Tissue-specific requirements of *Tcf12* for suture patency and calvarial bone growth

To investigate where *Tcf12* is required for suture development and skull bone growth, we deleted both copies of *Tcf12* in neural crest ($Tcf12^{flox/flox}$; *Wnt1-Cre*), mesoderm ($Tcf12^{flox/flox}$; *Mesp1-Cre*) or

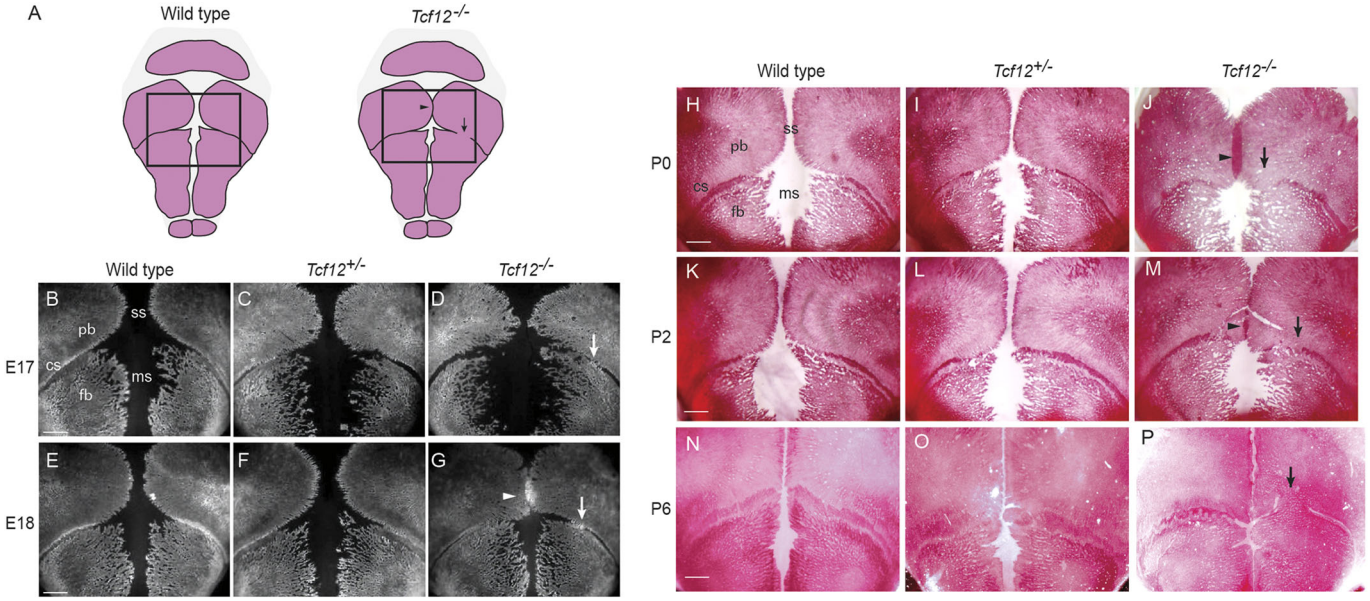

Fig. 1. Coronal suture fusion in *Tcf12* null mice. (A) Schematic of wild-type and $Tcf12^{-/-}$ skulls with bones in red. Boxes indicate regions of skull shown in B-P. (B-G) Skulls of embryonic mice stained with Alizarin Red S and imaged for fluorescence. See Movies 1 and 2. (H-P) Skulls of postnatal mice stained with Alizarin Red S. Arrows indicate coronal suture fusion and arrowheads indicate abnormal overlap of the sagittal suture. cs, coronal suture; fb, frontal bone; ms, metopic (frontal) suture; pb, parietal bone; ss, sagittal suture. See Table 1 for *n* values. Scale bars: 1 mm.

Development (2022) 149, dev199575. doi:10.1242/dev.199575

Table 1. Severity of craniosynostosis in different genetic combinations

Genotype	*n*	Coronal craniosynostosis index (C.I.)±s.e.m.	Penetrance %
Embryonic stages (E17-E18)			
Wild type	11	0.0±0.0	0
Tcf12$^{+/-}$	18	0.0±0.0	0
Tcf12$^{-/-}$	10	0.7±0.3	50
Postnatal stages (P0-P21)			
Wild type	15	0.0±0.0	0
Tcf12$^{+/-}$	17	0.0±0.0	0
Tcf12$^{-/-}$	22	0.5±0.2	36
Tcf12$^{flox/flox}$*; Wnt1-Cre; Mesp1-Cre*	6	1.7±1.8	66.7
Twist1$^{+/-}$	9	2.2±0.5	44
Tcf12$^{+/-}$*; Twist1*$^{+/-}$	6	4.8±0.4	100

Calvaria were dissected at the indicated developmental stages and stained with Alizarin Red S. The degree of fusion of the coronal suture was assessed as described by Oram and Gridley (2005).

both (*Tcf12*$^{flox/flox}$; *Wnt1-Cre*; *Mesp1-Cre*). Whereas homozygous loss of *Tcf12* in either neural crest or mesoderm alone did not affect coronal suture patency, loss in both tissues caused coronal suture fusion (Fig. 2A-H). The severity of coronal suture defects appeared to be higher in combined conditional mutants (coronal synostosis index 1.7±1.8; mean±s.e.m.) than in conventional homozygous *Tcf12* mice (coronal synostosis index 0.5±0.2), although the severity of synostosis was highly variable in combined conditional deletion mutants. Given a similar requirement for *Twist1* in both mesoderm- and neural crest-derived tissues (Teng et al., 2018), these results support *Tcf12* and *Twist1* acting together in the same tissues for coronal suture formation.

When *Tcf12* was deleted in the mesoderm, we observed an abnormal overlap of the parietal bones of the sagittal suture (Fig. 2C,D), consistent with accelerated growth of the mesoderm-derived parietal bones (Fig. 2C) and similar to what was seen in *Tcf12* nulls (Fig. 1G,J,M). Upon mesodermal deletion, we also observed an expansion of the size of the parietal bone relative to the neural crest-derived frontal bone at P21, effectively moving the coronal suture anteriorly (Fig. 2G,I). Reciprocally, the size of the frontal bone expanded relative to the parietal bone upon neural crest deletion of *Tcf12*, shifting the coronal suture posteriorly (Fig. 2F,I). This relative size change was associated with increased apical growth of the frontal bone compared with the parietal bone rudiments in *Tcf12*$^{flox/flox}$*; Wnt1-Cre* mice, and a trend toward increased parietal versus frontal bone rudiment growth in *Tcf12*$^{flox/flox}$*; Mesp1-Cre* mutants, as revealed by alkaline phosphatase (ALP) staining at E13.5 and E14.5 (Fig. 2J-P).

At E18.5 and P1, the apical expansion of the frontal bones in *Tcf12*$^{flox/flox}$; *Wnt1-Cre* mice was also associated with the appearance of Alizarin Red+ heterotopic bones in the normally unossified area when compared with controls (Fig. 3A-G). Sectioning of neural crest-derived mesenchyme (*Tcf12*$^{flox/flox}$*; Wnt1-Cre; R26RLacZ*) at E15.5 showed that the ectopic bone is entirely of neural crest origin (Fig. 3H-O). Thus, the expansion of the frontal relative to the parietal bone upon neural crest-specific *Tcf12* loss is due, at least in part, to accelerated osteoblast differentiation within neural crest-derived cells.

Table 2. Associated phenotypes of Tcf12 mutants

	Tcf12$^{-/-}$ (*n*=32)	*Twist*$^{+/-}$*; Tcf12*$^{+/-}$ (*n*=46)	*Twist*$^{+/-}$*; Tcf12*$^{-/-}$ (*n*=21)
Curly tail	12.5%	0%	19%
Exencephaly	3%	0%	33%
Open ventral body wall	0%	0%	14%

Non-suture phenotypes of mice of the indicated genotypes were scored at embryonic stages.

Reduction of *Tcf12* function affects osteoblast dynamics and asymmetric distribution of Grem1+ mesenchyme

We showed previously that closer apposition of frontal and parietal bones in *Twist1*$^{+/-}$*; Tcf12*$^{+/-}$ mutants was associated with increased proliferation yet reduced number of putative progenitors at the growing bone fronts and the developing coronal suture (Teng et al., 2018). Given the accelerated frontal and parietal bone growth we observed upon *Tcf12* deletion, we assessed whether osteoblast and progenitor dynamics were also altered in *Tcf12* null mice. At E14.5, we observed an ∼22% increase in the number of Sp7+ osteolineage cells along the frontal and parietal bone fronts of *Tcf12* mutants, yet the percentage of Sp7+ osteolineage cells incorporating bromodeoxyuridine (BrdU; a marker of cell proliferation) and the total number of proliferative Sp7− cells were unchanged (Fig. S1). These findings indicate that *Tcf12* and *Twist1* function in common to limit osteogenic commitment.

We next examined the number of putative osteoprogenitors at the developing coronal suture in *Tcf12* mutants. We had previously shown that Grem1+ cells, which function as skeletal stem cells in long bones (Worthley et al., 2015), were reduced in the coronal suture mesenchyme of *Tcf12*$^{+/-}$*; Twist1*$^{+/-}$ mice (Teng et al., 2018). Interestingly, we observed that Grem1+ cells were asymmetrically distributed around the bones at the forming coronal suture, with more Grem1+ cells above (i.e. closer to skin) than below (i.e. closer to brain) relative to the frontal bone, and conversely more Grem1+ cells below than above the parietal bone in wild types at E14.5 (Fig. 4A-G). This asymmetric distribution of Grem1+ cells in the ectocranial versus endocranial layers correlates with the parietal bone reproducibly overlapping above the frontal bone at the mature coronal suture. In *Tcf12* null mice, we observed selective reductions of Grem1+ cells above the frontal bone (Fig. 4A-G), resulting in a more symmetric arrangement of Grem1+ cells. Grem1+ cells above and below the parietal bone were also reduced in mutants. Consistently, we observed that *Tcf12* and, in particular, *Twist1* expression were also asymmetrically enriched in mesenchyme above versus below the frontal bone and below versus above the parietal bone tip at E15.5 (Fig. 4H-J, arrows). We also attempted to examine whether Grem1+ cell asymmetry was established earlier at E13.5, a stage before the parietal and frontal bones meet, but did not observe significant Grem1 expression at this stage. Instead, we examined the expression of *Six2*, which we had recently shown broadly labels coronal suture mesenchyme (Farmer et al., 2021). At E12.5 and E13.5, we observed more *Six2* expression above the frontal bone than above the parietal bone (*Six2* expression in the dura below the bones prevented us from assessing relative expression below the frontal and parietal bone) (Fig. 4K,L). These results indicate selective enrichment of Grem1+/Six2+ mesenchyme above the frontal bone compared with the parietal bone before these bones contact to form the coronal suture. The loss of asymmetry in *Tcf12* mutants further correlates with the frontal and parietal bones meeting end-on-end and often fusing.

Neural crest-mesoderm boundary defects in *Tcf12* null mice

Disruption of the boundary between the osteogenic neural crest cells of the frontal bone and the mesoderm-derived coronal suture mesenchyme was observed in *Twist1* heterozygous mice and was

Development (2022) 149, dev199575. doi:10.1242/dev.199575

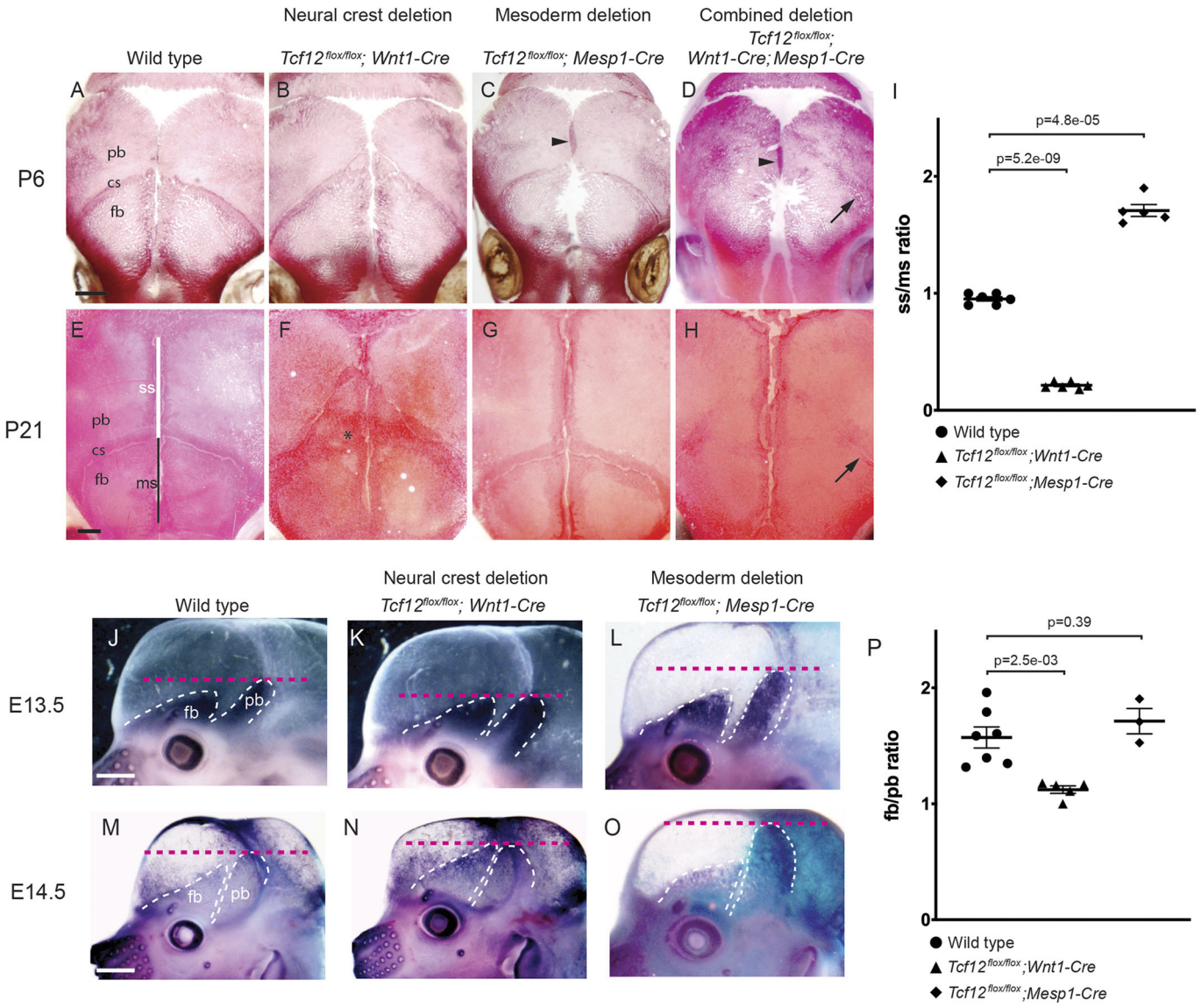

Fig. 2. Tissue-specific requirements of *Tcf12* in calvarial bone growth and suture patency. (A-H) Skulls of the indicated genotypes were stained with Alizarin Red S at P6 and P21. Note the change in the relative size of the frontal and parietal bones in *Tcf12*$^{flox/flox}$;*Wnt1-Cre* and *Tcf12*$^{flox/flox}$;*Mesp1-Cre* mutants. An abnormally overlapping sagittal suture (arrowheads) was apparent in both *Tcf12*$^{flox/flox}$; *Mesp1-Cre* and *Tcf12*$^{flox/flox}$; *Mesp1-Cre*; *Wnt1-Cre* (combined deletion) mutants. Asterisk marks area of thickened Alizarin staining, and arrows show a small amount of remaining coronal suture in combined deletion mutants. Wild type (*n*=6), *Tcf12*$^{flox/flox}$; *Wnt1-Cre* (*n*=6), *Tcf12*$^{flox/flox}$; *Mesp1-Cre* (*n*=5), *Tcf12*$^{flox/flox}$; *Mesp1-Cre*; *Wnt1-Cre* (*n*=4). (I) Quantification of the ratio of the sagittal suture (ss) to the metopic suture (ms) at P21 illustrates relative expansion of the frontal bone (low ss/ms ratio) and parietal bone (high ss/ms ratio) upon deletion of *Tcf12* from the neural crest or mesoderm lineages, respectively. *P*-values of comparisons were obtained from an unpaired two-tailed Student's *t*-test. Error bars represent s.e.m. (J-O) Lateral views of ALP staining of frontal and parietal bone rudiments (white dashed lines). Note apical expansion of the frontal bone rudiment in *Tcf12*$^{flox/flox}$;*Wnt1-Cre* embryos, and apical expansion of the parietal bone rudiment in *Tcf12*$^{flox/flox}$; *Mesp1-Cre* embryos. The red dotted lines indicate the apical extent of the expansion of the parietal bone primordia. The embryo shown in O carries the R26R allele and is stained for *lacZ* in blue. All experiments were performed at least in triplicate. (P) Quantification of the ratio of frontal bone area (fb) to parietal bone area (pb) highlights the relative expansion of the frontal bone (high fb/pb ratio) or parietal bone (low fb/pb ratio) upon deletion of *Tcf12* from the neural crest or mesoderm lineages, respectively. *P*-values of comparisons were obtained from an unpaired two-tailed Student's *t*-test. Error bars represent s.e.m. cs, coronal suture; fb, frontal bone; ms, metopic suture; pb, parietal bone; ss, sagittal suture. Scale bars: 1 mm.

accompanied by a reduction in Eph-ephrin signaling in the ectocranial layer above the coronal suture (Merrill et al., 2006). We used *Wnt1-Cre*; *R26R* mice to trace the fate of neural crest-derived cells at the coronal sutures of E13.5 embryos (Jiang et al., 2002). In wild types, *lacZ*+ neural crest-derived cells contributed to the frontal bone and were excluded from the mesoderm-derived coronal suture mesenchyme and parietal bone. In contrast, neural crest-derived cells invaded the coronal suture mesenchyme in *Tcf12*$^{-/-}$ mutants, consistent with a defect in the neural crest-mesoderm boundary (Fig. 5A-F). We next examined ephrinA2-EphA signaling in *Tcf12* null mice, as we had previously shown that this pathway is required in the ectocranial layer above the forming suture to regulate neural crest-derived cell migration and boundary formation (Merrill et al., 2006; Ting et al., 2009; Yen et al., 2010). In *Tcf12*$^{-/-}$ mutants, ectocranial expression of *Efna2* was completely abolished (Fig. 5G-J). We conclude that Tcf12 and Twist1 act similarly to regulate *Efna2* ectocranial expression and the boundary between osteogenic and non-osteogenic cells at the nascent coronal suture.

Development (2022) 149, dev199575. doi:10.1242/dev.199575

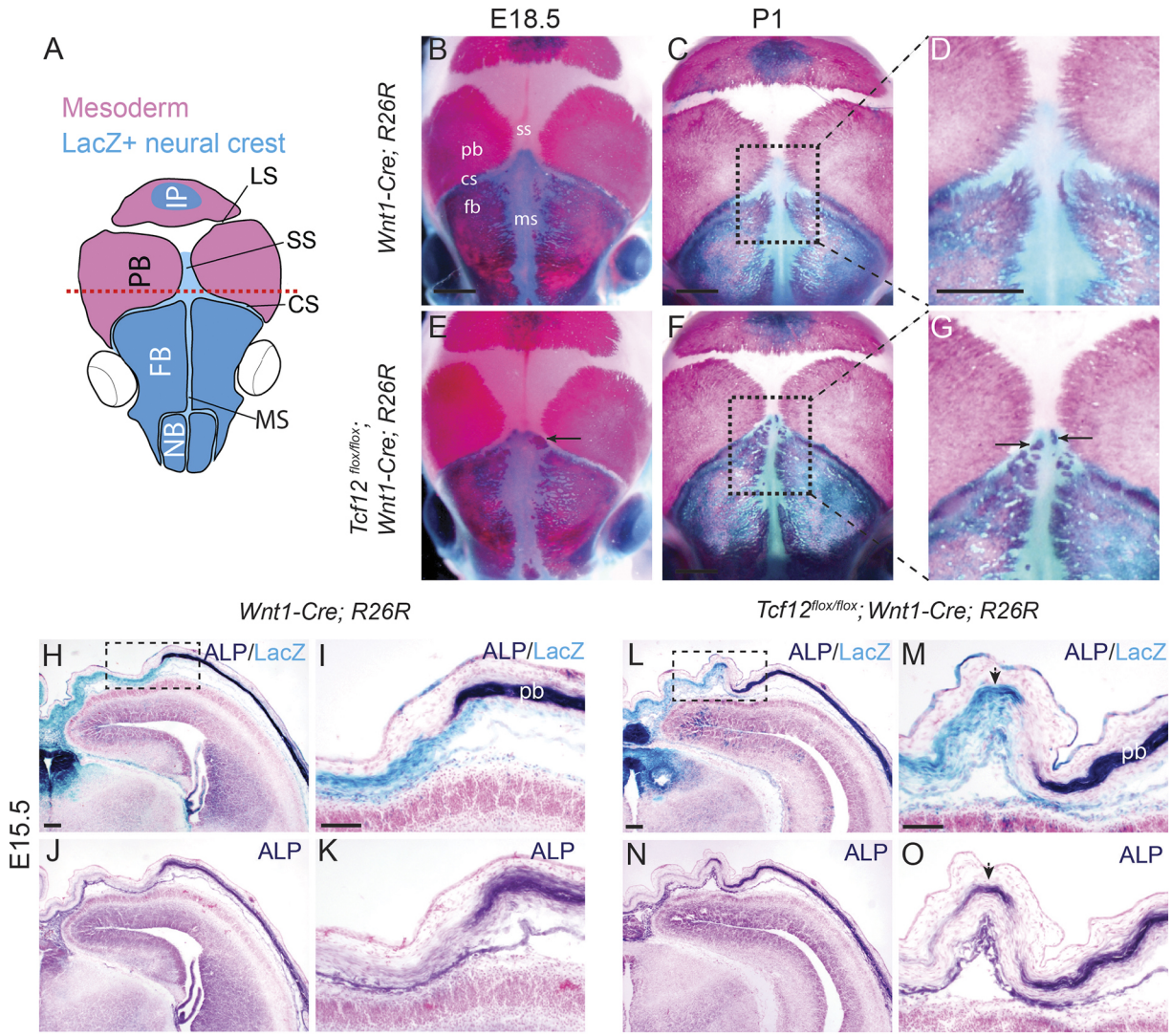

Fig. 3. Accelerated frontal bone formation upon neural crest deletion of *Tcf12*. (A) Schematic of *Wnt1*-Cre; *R26R* neonatal mouse skull with unlabeled mesoderm-derived bones in red and *lacZ*+ neural crest-derived bones and mesenchyme in blue. Red dotted line shows approximate location of sections. (B-G) Skulls of the indicated genotypes were stained with Alizarin Red S (red, bone) and for *lacZ* (blue, neural crest-derived cells) at E18.5 (B,E) or P1 (C,D,F,G). In all *Tcf12*$^{flox/flox}$; *Wnt1-Cre; R26R* animals (n=4 at E18.5, n=4 at P0), bony islands (arrows) were observed in *lacZ*+ neural crest-derived cells at the anterior border of the sagittal suture (E and F; G is magnification of boxed region of F). (H-O) Adjacent cross-sections of embryos of the indicated genotypes were stained for ALP (purple, osteoblasts) or *lacZ* (blue, neural crest-derived cells) at E15.5. Boxed areas correspond to enlarged regions on the right. Note the bony islands in adjacent sections shown in L and N are *lacZ*+. Ectopic ALP+ bone in the *lacZ*+ domain was observed in 3/3 mutants and 0/3 wild-type siblings from a heterozygous incross. cs, coronal suture; fb, frontal bone; ip, interparietal bone; ls, lambdoid suture; ms, metopic suture; nb, nasal bone; pb, parietal bone; ss, sagittal suture. Scale bars: 1 mm (B-G); 50 µm (H-O).

Tcf12 is largely dispensable in postnatal suture mesenchyme for suture patency

We next investigated potential roles for Tcf12 in regulating suture patency at postnatal stages. Using RNAscope *in situ* hybridization of 14-week-old mouse skulls, we observed postnatal expression of *Tcf12* throughout the mesenchyme of the coronal suture, as well as in periosteum above and dura mesenchyme below the suture (Fig. 6C). As the suture mesenchyme expression of *Tcf12* overlaps with the reported labeling by *Gli1-CreERT2* at 4 weeks after birth (Zhao et al., 2015), we treated *Gli1-CreERT2; Tcf12*$^{flox/flox}$ mice at this stage with tamoxifen to delete *Tcf12* in the postnatal suture mesenchyme. Four weeks after induction, micro-CT and histological analysis revealed no defects in the coronal suture when compared with untreated wild-type controls (Fig. 6A,B,D,E). At this same stage, *in situ* hybridization for *Tcf12* mRNA revealed an ~60% reduction in expression within the suture region, which likely includes non-skeletogenic cells not derived from Gli1+ skeletal stem cells (Fig. 6F-H). This finding argues against a major postnatal role of *Tcf12* in Gli1+ suture mesenchyme for maintaining suture patency, although we cannot rule out postnatal roles for *Tcf12* in cells outside of the Gli1+ domain.

DISCUSSION

The ability of heterozygous mutations in *TWIST1* or *TCF12* to cause coronal synostosis in Saethre-Chotzen syndrome, as well as genetic interactions of *Twist1* and *Tcf12* homologs in zebrafish and mice, had suggested that *Twist1* and *Tcf12* may similarly control several key processes in calvarial development. However, *Twist1* can also form homodimers, as well as heterodimers with other partners besides *Tcf12*, suggesting that there could be differences between

Development (2022) 149, dev199575. doi:10.1242/dev.199575

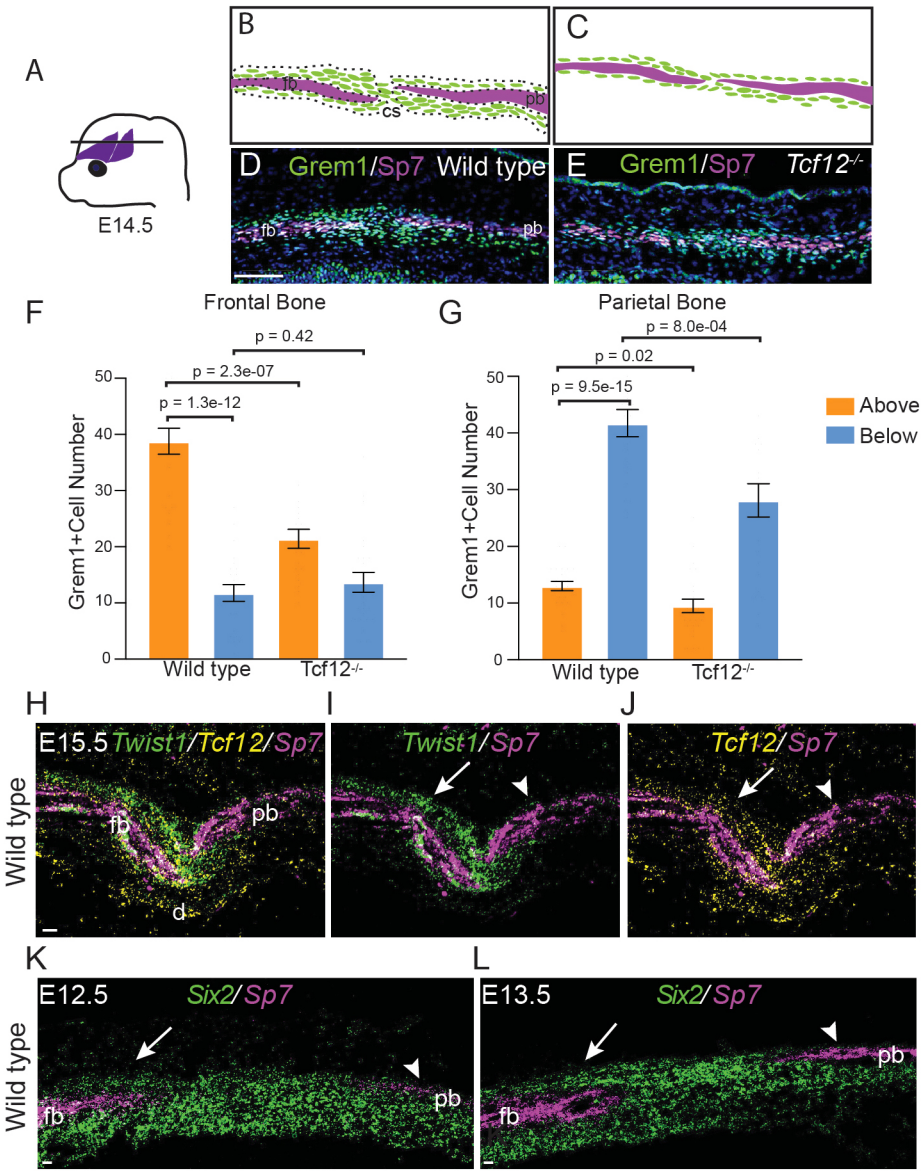

Fig. 4. Asymmetric distribution of mesenchyme around the developing frontal and parietal bone fronts. (A) Schematic of an embryonic mouse head showing the frontal and parietal bone rudiments. Line shows the plane of section for *in situ* analysis. (B-E) Immunostaining of sections through the coronal sutures of E14.5 embryos with antibodies against Grem1, a putative marker of osteoprogenitor cells, and Sp7, a marker of osteolineage cells (D,E). Diagrams of the bones (magenta) and associated mesenchyme (green) are shown above (B,C). Dotted lines in B show the four quadrants in which mesenchyme cell counting was performed. (F,G) Quantification of the Grem1+ cells in the dotted quadrants of the diagrams. Wild type (n=5); *Tc12*$^{-/-}$ (n=5); 4-6 sections per embryo. Error bars represent the s.e.m. *P*-values were calculated using an unpaired two-tailed Student's *t*-test with Bonferroni correction for multiple comparisons. (H-L) RNAscope *in situ* hybridization of the developing frontal and parietal bones and the coronal suture region. At E15.5, 3/3 wild types showed higher expression of *Tcf12* and *Twist1* above the frontal relative to the parietal bone. Similarly, 2/2 wild types at E12.5 and 2/2 wild types at E13.5 displayed greater *Six2* expression above the frontal relative to the parietal bone. *Sp7* labels osteoblasts in magenta. Arrows show greater expression above the frontal bone and arrowheads show lower expression above the parietal bone. cs, coronal suture; d, dural mesenchyme; fb, frontal bone; pb, parietal bone. Scale bars: 50 µm.

Twist1 and Tcf12 roles during coronal suture development. Here, we show that *Twist1*$^{+/-}$ and *Tcf12*$^{-/-}$ mutants share many, but not all, defects related to coronal suture formation, suggesting a primary role for Twist1-Tcf12 heterodimers in this process.

We find that *Tcf12*$^{-/-}$ mutants display the same partially penetrant coronal synostosis as *Twist1*$^{+/-}$ mutants, which is similarly preceded by accelerated frontal and parietal bone growth and disruption of the boundary between sutural and osteogenic cells (Merrill et al., 2006; Yen et al., 2010; Ting et al., 2009; Teng et al., 2018). The observation of coronal suture fusion by Alizarin Red staining as early as E17.5, as well as the similar penetrance and severity of suture defects at late embryonic and postnatal stages, points to defects in the formation as opposed to the maintenance of the coronal suture in *Tcf12*$^{-/-}$ mice. At a molecular level, this is reflected by an increase in Sp7+ osteolineage cells and a concomitant decrease in Grem1+ mesenchyme cells at embryonic bone fronts, in addition to loss of ectocranial *Efna2* expression. As with *Twist1*, *Tcf12* must be mutated in both the neural crest and mesoderm lineages to disrupt the coronal suture. These similarities suggest that Tcf12 and Twist1 may act together to control common gene targets and cellular processes that are important for proper coronal suture development. We did not, however, observe the same increases in osteoblast and/or progenitor proliferation in *Tcf12* mutants as reported for *Twist1*$^{+/-}$ mutants (Teng et al., 2018). This difference could be explained by the milder suture fusion seen in *Tcf12*$^{-/-}$ mutants, and/or a selective requirement of Twist1 homodimers for restricting the proliferative expansion of bone-forming cells.

Our results suggest several potential mechanisms that may lead to synostosis upon loss of *Tcf12* and/or *Twist1*. Mutation of either gene results in excess osteoblast production and acceleration of frontal and parietal bone growth. This is clearly seen upon inactivation of *Tcf12* in the neural crest. In these animals, small disorganized islands of bone form in the frontal fontanelle, the space in which the posterior portion of the parietal bones and anterior portion of the frontal bones come together. These bony islands arise from neural crest-derived cells of the frontal foramen, reminiscent of our previous findings that inactivation of *Msx1* and *Msx2* in neural crest causes inappropriate conversion of non-osteogenic neural crest-derived cells to osteoblasts (Roybal et al., 2010). Why only

Development (2022) 149, dev199575. doi:10.1242/dev.199575

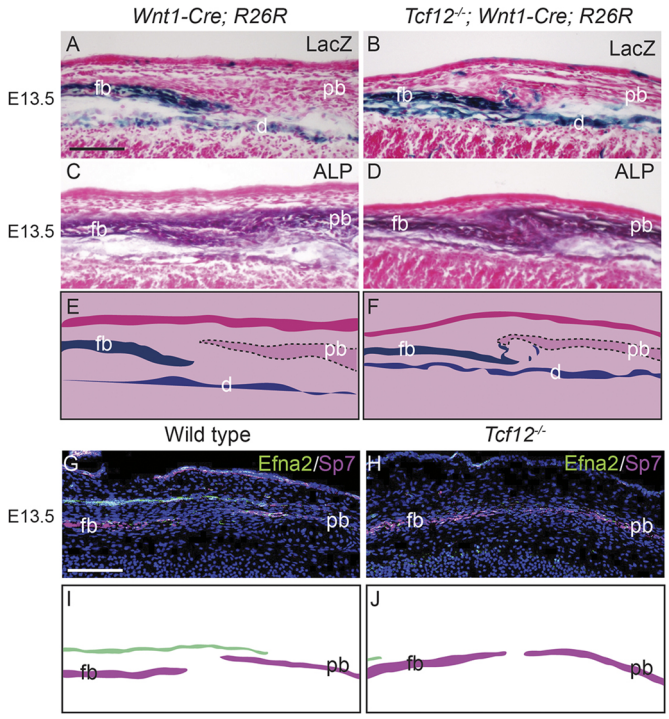

Fig. 5. Disruption of the neural crest-mesoderm boundary at the *Tcf12* mutant coronal suture. (A-J) Sections of wild-type *Wnt1-Cre*; *R26R* and *Tcf12*$^{-/-}$; *Wnt1-Cre*; *R26R* embryos at the level of the coronal suture were stained for *lacZ* (A,B), ALP (C,D), or antibodies for EfnA2 and Sp7 (G,H) at E13.5. In *Tcf12*$^{-/-}$ mutants, *lacZ*+ neural crest cells are located ectopically in the area of the prospective coronal suture (A,B, diagrammed in E,F, respectively), and Efna2 is lost in the ectocranial layer (G,H, diagrammed in I,J, respectively). All experiments were performed in triplicate with similar results. d, dural mesenchyme; fb, frontal bone; pb, parietal bone. Scale bars: 50 µm.

inactivation of *Tcf12* or *Twist1* in both the neural crest and mesoderm causes synostosis is unclear. In one model, stem cell depletion in one lineage can be compensated for by stem cells from the other lineage. Hence, depletion in both lineages would be required to bring stem cell numbers below the threshold necessary to maintain separate bones. Consistent with this model, we observe depletion of Grem1+ mesenchyme cells associated with the bone fronts in both *Twist1*$^{+/-}$ and *Tcf12*$^{-/-}$ mutants, though future lineage tracing will be required to determine whether Grem1+ cells act as osteogenic stem cells as described in the limbs (Worthley et al., 2015). In addition to acceleration of bone growth, disruption of either *Tcf12* or *Twist1* also results in a disruption of the boundary between the frontal bone and the suture mesenchyme that is associated with loss of overlying *Efna2*+ ectocranial expression. Whether this boundary defect is a secondary consequence of the accelerated bone growth, or is an independent phenotype that further contributes to synostosis, requires further investigation.

Further arguing for a largely embryonic role of Tcf12 in suture patency, deletion of *Tcf12* in Gli1-expressing cells of the 1 month postnatal coronal suture had no effect on suture maintenance one month later. A similar lack of postnatal suture phenotype was recently reported for mice in which *Twist1* was conditionally deleted by *Gli1-CreERT2* at similar stages (Yu et al., 2021). However, expression of *Tcf12* in the coronal suture and surrounding tissues was not completely eliminated in *Gli1-CreERT2; Tcf12*$^{flox/flox}$ mice following postnatal tamoxifen administration, potentially due to incomplete activity of CreERT2 and/or expression of *Tcf12* in some *Gli1-CreERT2*− lineage cells. Given the continued expression of *Tcf12* in coronal suture mesenchyme until at least 14 weeks after birth, future experiments using different tools to completely eliminate postnatal Tcf12 function will be needed to better assess requirements for *Tcf12* after birth.

Our results also provide a potential explanation for the overlap of the frontal and parietal bones at the coronal suture. Unlike the medially placed interfrontal and sagittal sutures, which are formed by the direct apposition of osteogenic fronts on a level plane, the transversely situated coronal suture is reproducibly formed by the parietal bone overlapping above the frontal bone. In wild types, we find a preferential enrichment of Grem1+/Six2+ mesenchyme cells above the frontal bone and below the parietal bone, similar to *Tcf12* and *Twist1* expression and our recent reports of *Erg* expression (Farmer et al., 2021). We find that enrichment of *Six2* above the frontal but not above the parietal bone begins as early as E12.5, when the bones are still distant from one another. One possibility is that these asymmetries skew the growth of the two bones off their central axes such that the parietal reproducibly overlaps above the frontal bone. In mice deficient for *Tcf12* or *Twist1*, the osteogenic fronts of the frontal and parietal bones fail to overlap, and this correlates with a more symmetrical distribution of Grem1+ cells (this study) and Six2+/Erg+ cells (Farmer et al., 2021) above and below the growing frontal bone. In contrast, distribution around the parietal bone was less affected. One explanation for the reduction in frontal but not parietal bone mesenchymal asymmetry is loss of the *Efna2*+ ectocranial layer in mutants. The ectocranial *Efna2*+ layer overlays the enriched Grem1+/Six2+ cells of the frontal bone but does not significantly extend into the parietal side of the coronal suture. It is therefore possible that the ectocranial layer serves to enrich Grem1+/Six2+ mesenchyme above the frontal bone in normal animals, with loss of this ectocranial layer in mutants disrupting asymmetry and leading to increased apposition of bone fronts that could further contribute to synostosis.

In summary, our study points to similar roles for Twist1 and Tcf12 in controlling embryonic processes essential for coronal suture formation, thus explaining why Saethre-Chotzen syndrome can be caused by heterozygous inactivating mutations in either *TWIST1* or *TCF12*. The similarities of defects in heterozygous *Twist1* and homozygous *Tcf12* mutant mice further support the model that Twist1 and Tcf12 function as heterodimers to control unique sets of genes important for regulation of osteoblast progenitors. Future experiments will be required to identify genomic regions specifically bound by such heterodimers, as well as the molecular and cellular mechanisms by which these transcription factors regulate the timing and rate of calvarial bone addition to ensure proper coronal suture formation.

MATERIALS AND METHODS

Mouse mutants and genotyping

The Institutional Animal Care and Use Committee of the University of Southern California approved all animal experiments (Protocol 20552). We did not separate mice for experiments by gender, and wild-type and mutant mice were maintained on a C57BL/6 background. The *Tcf12* (Wojciechowski et al., 2007), *Twist1* (Chen and Behringer, 1995), *R26R* (Soriano, 1999), *Wnt1-Cre* (Danielian et al., 1998), *Mesp1-Cre* (Saga et al., 1999) and *Gli1-CreERT2* (Zhao et al., 2015) alleles were genotyped by PCR as described. *Gli1-CreERT2; Tcf12-fl/fl* mice were injected intraperitoneally with 20 mg/ml tamoxifen in corn oil (Sigma-Aldrich, C8267) for three consecutive days starting at 1 month of age as previously described (Yu et al., 2021).

Rationale for choice of developmental stages for analysis

Craniosynostosis is most easily assessed at postnatal stages (e.g. Yen et al., 2010). Because *Tcf12* homozygous mutants often die perinatally

Development (2022) 149, dev199575. doi:10.1242/dev.199575

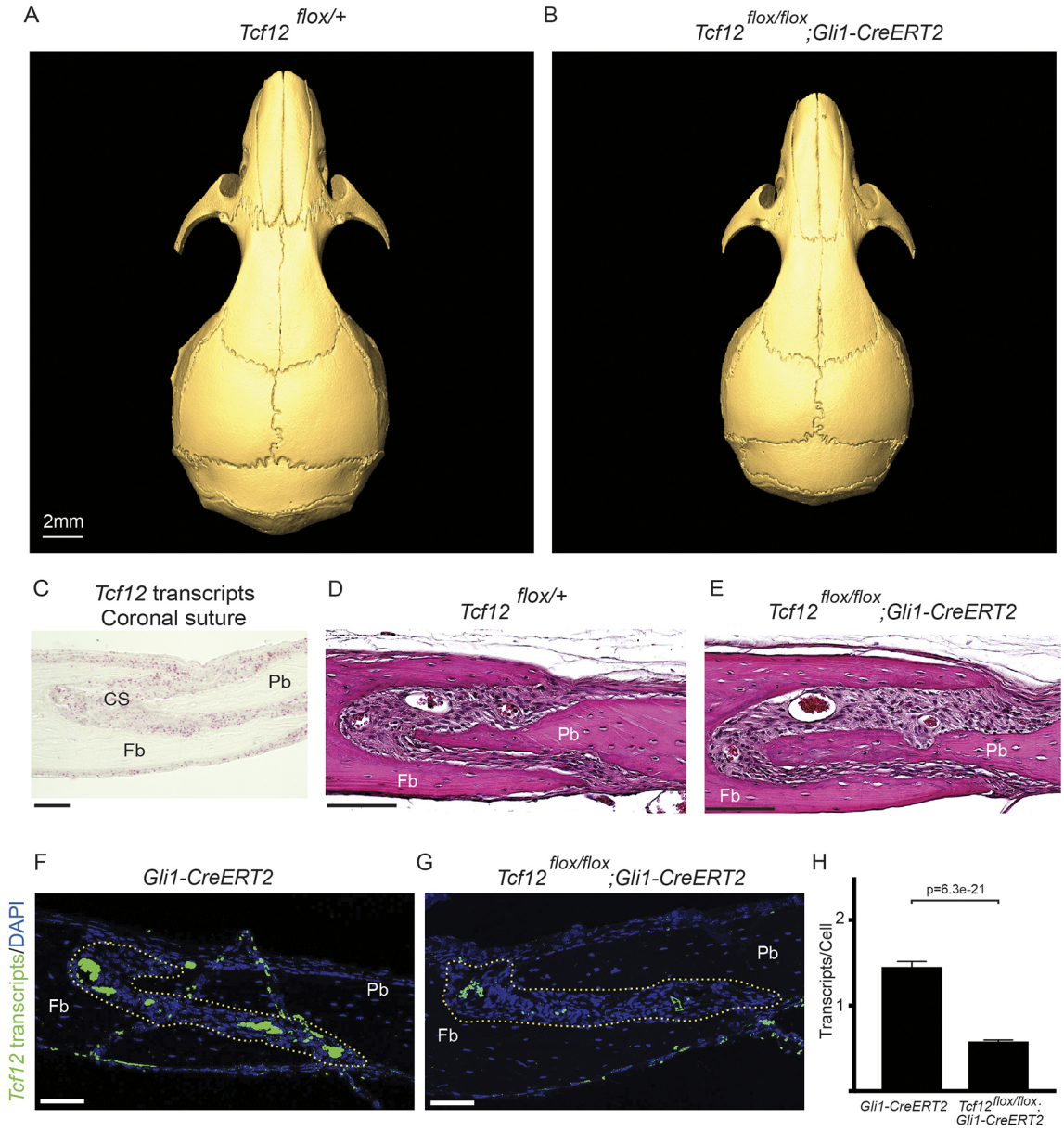

Fig. 6. Postnatal deletion of *Tcf12* in Gli1+ suture mesenchyme does not affect coronal suture maintenance. (A,B) 3D reconstructed microCT images of *Tcf12*$^{flox/+}$ (*n*=2) and *Tcf12*$^{flox/flox}$; *Gli1-CreERT2* (*n*=2) calvaria. Sutures remained patent in both *Tcf12*$^{flox/flox}$; *Gli1-CreERT2* mice. (C) RNAscope *in situ* hybridization on sections of 14-week postnatal mice shows expression of *Tcf12* (red dots) in the coronal suture mesenchyme, as well as periosteum (above bones) and dura (below bones). (D,E) Sections through the coronal suture of *Tcf12*$^{flox/+}$ littermate controls (*n*=2) and *Tcf12*$^{flox/flox}$; *Gli1-CreERT2* mice (*n*=2) stained with H&E. (F,G) Fluorescent RNAscope *in situ* hybridization on sections of *Gli1-CreERT2* (*n*=2) and *Tcf12*$^{flox/flox}$; *Gli1-CreERT2* (*n*=2) mouse shows reduction of *Tcf12* transcripts (magenta) in conditional mutants. Yellow dotted outlines highlight suture mesenchyme defined for quantification. (H) Quantification of the number of *Tcf12* transcripts per cell in *Gli1-CreERT2* and *Tcf12*$^{flox/flox}$; *Gli1-CreERT2* mice reveals significant reduction in the number of *Tcf12* transcripts after tamoxifen treatment (*n*=2 per condition). For all experiments, tamoxifen was administered at 1 month after birth and skulls were analyzed at 2 months of age. Cs, coronal suture; Fb, frontal bone; Pb, parietal bone. Scale bars: 2mm (A,B); 50 µm (C-G).

(before P6), we typically used P0 animals. Some mice survived into the first postnatal week, and very rarely until P21. When we obtained such mice, we scored them for craniosynostosis and made them a part of our analysis. We also used embryonic stages to assess early events of suture development. At E14-E15, the frontal and parietal bone rudiments are coming into apposition and osteogenic cells and putative osteogenic stem cells are identifiable by marker gene expression (Ting et al., 2009; Yen et al., 2010; Teng et al., 2018; this study).

Whole-mount skull Alizarin Red S staining and microCT imaging

Skulls of newborn (P0) and postnatal mice were stained for bone with 2% Alizarin Red S in 1% KOH for 3-5 days. The specimens were then cleared and stored in 100% glycerol. Embryonic skulls were stained with 2% Alizarin Red S in phosphate buffered saline (PBS) for 1 h, destained for 1 h and imaged using a Leica MZ12.5 dissecting microscope. MicroCT imaging of postnatal skulls was performed using identical conditions as previously described (Yu et al., 2021).

Whole-mount ALP and *lacZ* staining

E13.5 and E14.5 heads were fixed in 4% paraformaldehyde (PFA) in PBS, and these were then bisected midsagitally after fixation. Presumptive calvarial bones were stained with NBT and BCIP (Roche, 11681451001). To detect *lacZ*, skulls of late-stage embryos were fixed in cold 4% PFA for

Development (2022) 149, dev199575. doi:10.1242/dev.199575

30 min followed by PBS washes. Calvarial bones were then stained with β-galactosidase staining solution overnight at 37°C.

Histology and immunohistochemistry

BrdU labeling to assess cellular proliferation at E14.5 was carried out as previously described (Teng et al., 2018). BrdU (Sigma-Aldrich, B9285) was injected into pregnant females (200 µg/g body weight) 2 h before dissection. Heads of embryos were embedded in Optimal Cutting Temperature (OCT) medium (VMR, 25608-930) before sectioning. Frozen sections were cut at 10 µm. Immunohistochemistry was performed using rat anti-BrdU (Bio-Rad Laboratories, MCA2060, 1:1200), rabbit anti-Sp7/Osx (Santa Cruz Biotechnology, sc-22536-r, 1:500), rabbit anti-ephrin-A2 (Santa Cruz Biotechnology, sc-912, 1:200) and goat anti-Grem1 (Thermo Fisher Scientific, PA5-47973, 1:40) diluted in 1% bovine serum albumin (BSA)/PBS and incubated overnight at 4°C. Detection of primary antibody of anti-Brdu, anti-Osx, anti-ephrinA2 and anti-Grem1 was performed by incubating goat anti-rat FITC (Santa Cruz Biotechnology, sc-2011, 1:150), goat anti-rabbit Alexa Fluor 568 (Abcam, ab1175471, 1:500), donkey anti-rabbit Alexa Fluor 568 (Abcam, ab1175470, 1:200) and donkey anti-goat IgG-Alexa Fluor 488 (Abcam, ab150129, 1:1200), respectively, for 1 h at room temperature followed by 4,6-diamidino-2-phenylindole (DAPI) counterstaining and examination by epifluorescence microscopy. Analysis of β-galactosidase activity of *Wnt1-Cre/R26R* reporter gene expression was carried out as previously described (Merrill et al., 2006). Postnatal calvaria were dissected and fixed in 10% neutralized buffered formalin (NBF, Sigma-Aldrich, HT501128) overnight at room temperature, then decalcified with 10% EDTA in 1× PBS for 1-14 days based on mouse age. Decalcified calvaria were dehydrated and embedded in paraffin. Tissue blocks were sectioned at 5 µm using a microtome (Leica) and mounted on SuperFrost Plus slides (Fisher, 12-550-15). Hematoxylin and Eosin (H&E) staining was completed following standard protocols.

RNAscope *in situ* hybridization

For postnatal calvaria, tissues were fixed in 10% NBF overnight at room temperature, decalcified with diethyl pyro carbonate (DEPC)-treated 10% EDTA in 1× PBS at 4°C, dehydrated sequentially with 15% sucrose in 1× PBS (4°C, overnight) and 30% sucrose in 1× PBS/OCT (4°C, overnight), and embedded in OCT on liquid nitrogen immediately. Frozen tissue blocks were sectioned at 8 µm on a cryostat (Leica, CM3050S) and mounted on SuperFrost Plus slides. Probes were purchased from Advanced Cell Diagnostics: *Tcf12* (504861); *Twist1* (414701-C2); *Six2* (500011); *Sp7* (403401-C3). Colorimetric *in situ* RNA detection was performed using RNAscope® 2.5 HD Detection Reagent (Advanced Cell Diagnostics, 322360) according to instructions provided by the manufacturer. Fluorescent RNAscope *in situ* hybridization for embryonic and adult time points was performed with the RNAscope Multiplex Fluorescent Kit v2 (Advanced Cell Diagnostics, 323100) according to the manufacturer's protocol for the fixed-frozen sections. Heat antigen retrieval was omitted for embryonic tissue to maximize nuclei quality, and TSA® Plus (PerkinElmer Fluorescein, NEL741001KT; Cy3, NEL744001KT; Cy5, NEL745001KT) reagents were used at 1:750 dilution. As the exon 18 deleted transcripts of the *Tcf12-flox* allele still retain some sequence recognized by the *Tcf12* RNAscope probe, the 60% reduction of *Tcf12* transcripts in tamoxifen-treated *Gli1-CreERT2*; $Tcf12^{flox/flox}$ animals may be an underestimate of deletion efficiency in the postnatal suture mesenchyme.

Quantitative and statistical analyses of craniosynostosis and related defects

The severity of coronal synostosis was quantified using a scoring method adapted from Oram and Gridley's craniosynostosis index (Oram and Gridley, 2005; Yen et al., 2010) applied specifically to the coronal suture (Teng et al., 2018). For each skull, the two coronal sutures were scored. The extent of fusion was assessed microscopically (0: unfused; 1: <50% fused; 2: ≥50% fused; 3: 100% fused). Scores for left and right sutures were added. Thus, for example, the maximum score given to two coronal sutures is 6. Phenotypic scoring was performed blinded to genotype. Comparisons among genotypes were analyzed by an unpaired two-tailed Student's *t*-test. For the measurement of coronal suture position, and hence the relative proportions of the parietal and frontal bones, we took the ratio of the sagittal suture to the metopic suture. The sagittal suture was defined as the distance between the juncture of the sagittal and lambdoid suture and the juncture of the sagittal and coronal suture. The metopic suture was defined as the distance between the juncture of the metopic and coronal suture and the anterior end of the frontal bones. For the measurement of frontal and parietal bone size at embryonic stages, the area of developing bones were quantified by outlining bones using ImageJ software and normalizing the size to that of the neighboring eye (Table S1). For assessment of BrdU+, Sp7+ and Grem1+ cells in mouse coronal suture area, stained-positive cells in a defined area along the bone fronts were manually counted (Tables S2 and S3). Four to five sections from the medial to lateral aspects of the coronal suture were quantified per animal and averaged. Comparisons were analyzed by an unpaired two-tailed Student's *t*-test, and the *P*-values were corrected for multiple testing with Bonferroni correction. For quantification of RNAscope signal, sutures were defined as all cells between neighboring frontal and parietal bones. Individual foci were defined as single transcripts, and each transcript was assigned to the nearest DAPI+ nucleus by manually counting in ImageJ (Table S4). Comparison of transcript count per cell was analyzed by an unpaired two-tailed Student's *t*-test. GraphPad Prism v8 was used for statistical analyses.

Acknowledgements

We thank members of the Maxson, Crump and Chai labs for helpful discussions.

Competing interests

The authors declare no competing or financial interests.

Author contributions

Conceptualization: M.T., D.T.F., C.S.T., Y.C., J.G.C., R.E.M.; Validation: M.T., D.T.F.; Formal analysis: M.T., D.T.F., C.S.T.; Investigation: M.T., D.T.F., C.S.T., J.H.; Writing - original draft: M.T., D.T.F., C.S.T., J.G.C., R.E.M.; Writing - review & editing: D.T.F., Y.C., J.G.C., R.E.M.; Supervision: Y.C., J.G.C., R.E.M.; Project administration: D.T.F., J.G.C., R.E.M.; Funding acquisition: D.T.F., C.S.T., Y.C., J.G.C., R.E.M.

Funding

This work was supported by National Institutes of Health (NIH) grant R01DE026339 (to R.E.M., J.G.C. and Y.C.), and NIH grant R35DE027550 (to J.G.C.). C.S.T. was supported by NIH training fellowships F31DE024031 and T90DE021982, and D.T.F. was supported by the Howard Hughes Medical Institute Hanna H. Gray Fellows Program and the Burroughs Wellcome Fund. Deposited in PMC for release after 12 months.

Peer review history

The peer review history is available online at https://journals.biologists.com/dev/article-lookup/doi/10.1242/dev.199575.

References

Chen, Z.-F. and Behringer, R. R. (1995). Twist is required in head mesenchyme for cranial neural tube morphogenesis. *Genes Dev.* **9**, 686-699. doi:10.1101/gad.9.6.686

Connerney, J., Andreeva, V., Leshem, Y., Muentener, C., Mercado, M. A. and Spicer, D. B. (2006). Twist1 dimer selection regulates cranial suture patterning and fusion. *Dev. Dyn.* **235**, 1345-1357. doi:10.1002/dvdy.20717

Danielian, P. S., Muccino, D., Rowitch, D. H., Michael, S. K. and McMahon, A. P. (1998). Modification of gene activity in mouse embryos in utero by a tamoxifen-inducible form of Cre recombinase. *Curr. Biol.* **8**, 1323-1326. doi:10.1016/S0960-9822(07)00562-3

El Ghouzzi, V., Le Merrer, M., Perrin-Schmitt, F., Lajeunie, E., Benit, P., Renier, D., Bourgeois, P., Bolcato-Bellemin, A.-L., Munnich, A. and Bonaventure, J. (1997). Mutations of the TWIST gene in the Saethre-Chotzen syndrome. *Nat. Genet.* **15**, 42-46. doi:10.1038/ng0197-42

Fan, X., Waardenberg, A. J., Demuth, M., Osteil, P., Sun, J. Q. J., Loebel, D. A. F., Graham, M., Tam, P. P. L. and Fossat, N. (2020). TWIST1 Homodimers and heterodimers orchestrate lineage-specific differentiation. *Mol. Cell Biol.* **40**, e00663-e00619. doi:10.1128/MCB.00663-19

Farmer, D. T., Mlcochova, H., Zhou, Y., Koelling, N., Wang, G., Ashley, N., Bugacov, H., Chen, H. J., Parvez, R., Tseng, K. C. et al. (2021). The developing mouse coronal suture at single-cell resolution. *Nat. Commun.* **12**, 4797. doi:10.1038/s41467-021-24917-9

Howard, T. D., Paznekas, W. A., Green, E. D., Chiang, L. C., Ma, N., Ortiz de Luna, R. I., Garcia Delgado, C., Gonzalez-Ramos, M., Kline, A. D. and Jabs,

E. W. (1997). Mutations in TWIST, a basic helix-loop-helix transcription factor, in Saethre-Chotzen syndrome. *Nat. Genet.* **15**, 36-41. doi:10.1038/ng0197-36

Jabs, E. W. (2008). TWIST and the Saethre-Chotzen syndrome. In *Inborn Errors of Development. The Molecular Basis of Clinical Disorders of Morphogenesis*, 2nd edn (ed. C. J. Epstein, R. P. Erickson and A. Wynshaw-Boris), pp. 474-481. Oxford, England: Oxford University Press.

Jiang, X., Choudhary, B., Merki, E., Chien, K. R., Maxson, R. E. and Sucov, H. M. (2002). Normal fate and altered function of the cardiac neural crest cell lineage in retinoic acid receptor mutant embryos. *Mech. Dev.* **117**, 115-122. doi:10.1016/S0925-4773(02)00206-X

Johnson, D. and Wilkie, A. O. (2011). Craniosynostosis. *Eur. J. Hum. Genet.* **19**, 369-376. doi:10.1038/ejhg.2010.235

Lajeunie, E., Le Merrer, M., Bonaïti-Pellie, C., Marchac, D. and Renier, D. (1995). Genetic study of nonsyndromic coronal craniosynostosis. *Am. J. Med. Genet.* **55**, 500-504. doi:10.1002/ajmg.1320550422

Lakso, M., Pichel, J. G., Gorman, J. R., Sauer, B., Okamoto, Y., Lee, E., Alt, F. W. and Westphal, H. (1996). Efficient in vivo manipulation of mouse genomic sequences at the zygote stage. *Proc. Natl. Acad. Sci. U. S. A* **93**, 5860-5865. doi:10.1073/pnas.93.12.5860

Massari, M. E. and Murre, C. (2000). Helix-loop-helix proteins: regulators of transcription in eucaryotic organisms. *Mol. Cell Biol.* **20**, 429-440. doi:10.1128/MCB.20.2.429-440.2000

Merrill, A. E., Bochukova, E. G., Brugger, S. M., Ishii, M., Pilz, D. T., Wall, S. A., Lyons, K. M., Wilkie, A. O. and Maxson, R. E.Jr. (2006). Cell mixing at a neural crest-mesoderm boundary and deficient ephrin-Eph signaling in the pathogenesis of craniosynostosis. *Hum. Mol. Genet.* **15**, 1319-1328. doi:10.1093/hmg/ddl052

Oram, K. F. and Gridley, T. (2005). Mutations in snail family genes enhance craniosynostosis of Twist1 haplo-insufficient mice: implications for Saethre-Chotzen Syndrome. *Genetics* **170**, 971-974. doi:10.1534/genetics.105.041277

Roybal, P. G., Wu, N. L., Sun, J., Ting, M. C., Schafer, C. A. and Maxson, R. E. (2010). Inactivation of Msx1 and Msx2 in neural crest reveals an unexpected role in suppressing heterotopic bone formation in the head. *Dev. Biol.* **343**, 28-39. doi:10.1016/j.ydbio.2010.04.007

Saga, Y., Miyagawa-Tomita, S., Takagi, A., Kitajima, S., Miyazaki, J. I. and Inoue, T. (1999). MesP1 is expressed in the heart precursor cells and required for the formation of a single heart tube. *Development* **126**, 3437-3447. doi:10.1242/dev.126.15.3437

Sharma, V. P., Fenwick, A. L., Brockop, M. S., McGowan, S. J., Goos, J. A., Hoogeboom, A. J., Brady, A. F., Jeelani, N. O., Lynch, S. A., Mulliken, J. B. et al. (2013). Mutations in TCF12, encoding a basic helix- loop-helix partner of TWIST1, are a frequent cause of coronal craniosynostosis. *Nat. Genet.* **45**, 304-307. doi:10.1038/ng.2531

Soriano, P. (1999). Generalized lacZ expression with the ROSA26 Cre reporter strain. *Nat. Genet.* **21**, 70-71. doi:10.1038/5007

Teng, C. S., Ting, M. C., Farmer, D. T., Brockop, M., Maxson, R. E. and Crump, J. G. (2018). Altered bone growth dynamics prefigure craniosynostosis in a zebrafish model of Saethre- Chotzen syndrome. *Elife* **7**, e37024. doi:10.7554/eLife.37024

Teng, C. S., Cavin, L., Maxson, R. E.Jr., Sánchez-Villagra, M. R. and Crump, J. G. (2019). Resolving homology in the face of shifting germ layer origins: lessons from a major skull vault boundary. *Elife* **8**, e52814. doi:10.7554/eLife.52814

Ting, M.-C., Wu, N. L., Roybal, P. G., Sun, J., Liu, L., Yen, Y. and Maxson, R. E.Jr. (2009). EphA4 as an effector of Twist1 in the guidance of osteogenic precursor cells during calvarial bone growth and in craniosynostosis. *Development* **136**, 855-864. doi:10.1242/dev.028605

Twigg, S. R. and Wilkie, A. O. (2015). A Genetic-Pathophysiological Framework for craniosynostosis. *Am. J. Hum. Genet.* **97**, 359-377. doi:10.1016/j.ajhg.2015.07.006

van Straaten, H. W. and Copp, A. J. (2001). Curly tail: a 50-year history of the mouse spina bifida model. *Anat. Embryol.* **203**, 225-237. doi:10.1007/s004290100169

Wang, L. H. and Baker, N. E. (2015). E Proteins and ID proteins: helix-loop-helix partners in development and disease. *Dev. Cell.* **35**, 269-280. doi:10.1016/j.devcel.2015.10.019

Wilkie, A. O. (1997). Craniosynostosis: genes and mechanisms. *Hum. Mol. Genet.* **6**, 1647-1656. doi:10.1093/hmg/6.10.1647

Wilkie, A. O., Bochukova, E. G., Hansen, R. M., Taylor, I. B., Rannan-Eliya, S. V., Byren, J. C., Wall, S. A., Ramos, L., Venâncio, M., Hurst, J. A. et al. (2006). Clinical dividends from the molecular genetic diagnosis of craniosynostosis. *Am. J. Med. Genet. A.* **140**, 2631-2639. doi:10.1002/ajmg.a.31366

Wojciechowski, J., Lai, A., Kondo, M. and Zhuang, Y. (2007). E2A and HEB are required to block thymocyte proliferation prior to pre-TCR expression. *J. Immunol.* **178**, 5717-5726. doi:10.4049/jimmunol.178.9.5717

Worthley, D. L., Churchill, M., Compton, J. T., Tailor, Y., Rao, M., Si, Y., Levin, D., Schwartz, M. G., Uygur, A., Hayakawa, Y. et al. (2015). Gremlin 1 identifies a skeletal stem cell with bone, cartilage, and reticular stromal potential. *Cell* **160**, 269-284. doi:10.1016/j.cell.2014.11.042

Yen, H. Y., Ting, M. C. and Maxson, R. E. (2010). Jagged1 functions downstream of Twist1 in the specification of the coronal suture and the formation of a boundary between osteogenic and non-osteogenic cells. *Dev. Biol.* **347**, 258-270. doi:10.1016/j.ydbio.2010.08.010

Yu, M., Ma, L., Yuan, Y., Ye, X., Montagne, A., He, J., Ho, T.-V., Wu, Y., Zhao, Z., Sta Maria, N. et al. (2021). Cranial suture regeneration mitigates skull and neurocognitive defects in craniosynostosis. *Cell.* **184**, 243-256. doi:10.1016/j.cell.2020.11.037

Zhao, H., Feng, J., Ho, T.-V., Grimes, W., Urata, M. and Chai, Y. (2015). The suture provides a niche for mesenchymal stem cells of craniofacial bones. *Nat. Cell Biol.* **17**, 386-396. doi:10.1038/ncb3139

Zhuang, Y., Cheng, P. and Weintraub, H. (1996). B-lymphocyte development is regulated by the combined dosage of three basic helix-loop-helix genes, E2A, E2-2, and HEB. *Mol. Cell Biol.* **16**, 2898-2905. doi:10.1128/MCB.16.6.2898

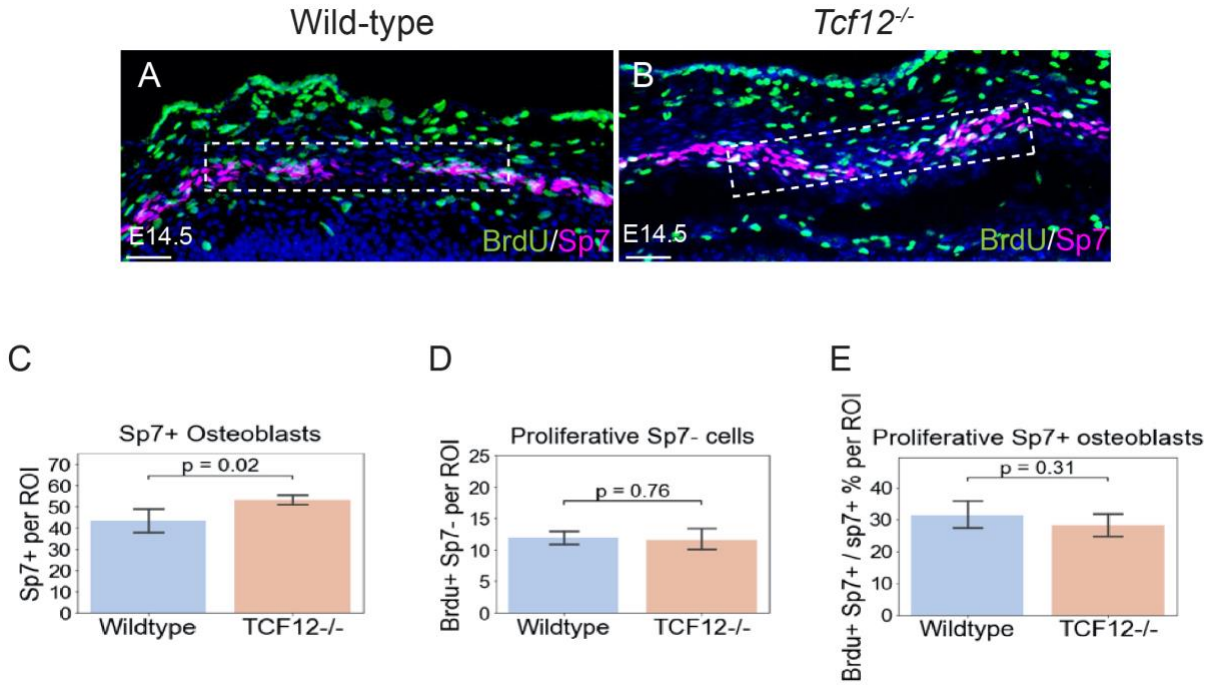

Fig. S1. Osteogenic cell dynamics in the *Tc12*$^{-/-}$ coronal suture. (A, B) Sections of E14.5 embryonic heads stained with antibodies against Sp7 and BrdU, after injecting BrdU into pregnant females two hours prior to harvesting embryos. Counts were performed in the boxed areas, which include the osteogenic fronts of the frontal and parietal bones and the interposed mesenchyme. Wild type: n = 5; *Tc12*$^{-/-}$: n = 6; 5-6 sections each embryo. (C-E) Quantification of Sp7+ osteolineage cells, proliferative Sp7-/BrdU+ cells, and proliferative Sp7+/BrdU+ cells in the boxed regions. Error bars represent the standard error of the mean. P values were calculated using an unpaired two-tailed Student's t-test. Scale bars = 50 μm.

Development • Supplementary information

Table S1. Bone size quantification of conditional *Tcf12*$^{flox/flox}$ mice with Mesp1:Cre or Wnt1:Cre.

Click here to download Table S1

Table S2. Sp7 and BrdU^{+} cell count at wild-type and Tcf12$^{-/-}$ coronal sutures.

Click here to download Table S2

Table S3. Gem1^{+} cell count in wild-type and Tcf12$^{-/-}$ coronal sutures.

Click here to download Table S3

Table S4. Manual count of Transcript number/nucleus in Gli1-CreERT2 (*n*=2) and Tcf12$^{flox/flox}$; Gli1-CreERT2 for *n*=2.

Click here to download Table S4

Development • Supplementary information

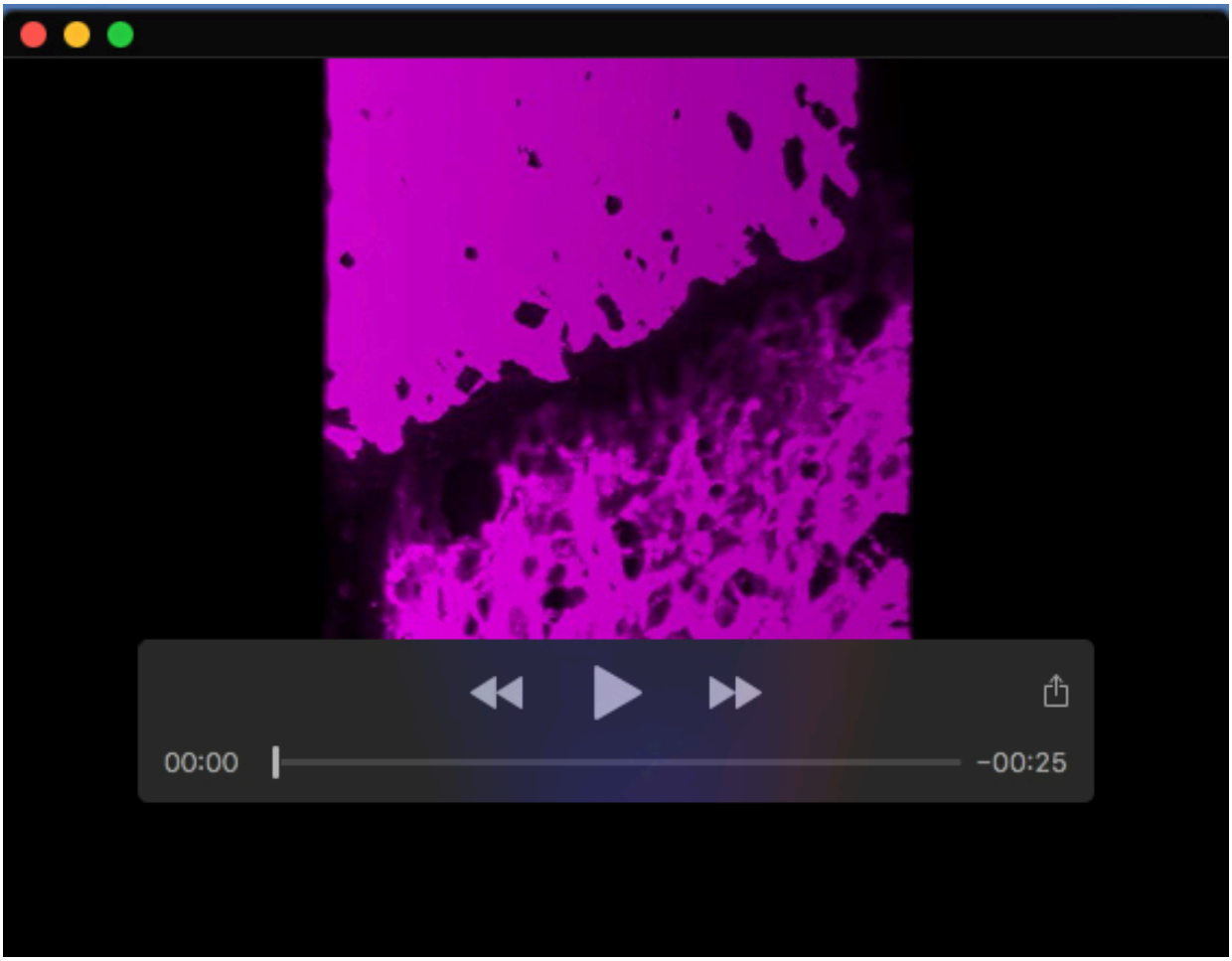

Movie 1. Projection of patent region of coronal suture from a Tcf12$^{+/-}$ mouse. 3D Confocal projection of an Alizarin Red-stained Tcf12$^{+/-}$ skull at the coronal suture. The frontal (bottom) and parietal bone (top) is separated by the Alizarin Red-negative zone of suture mesenchyme.

Development • Supplementary information

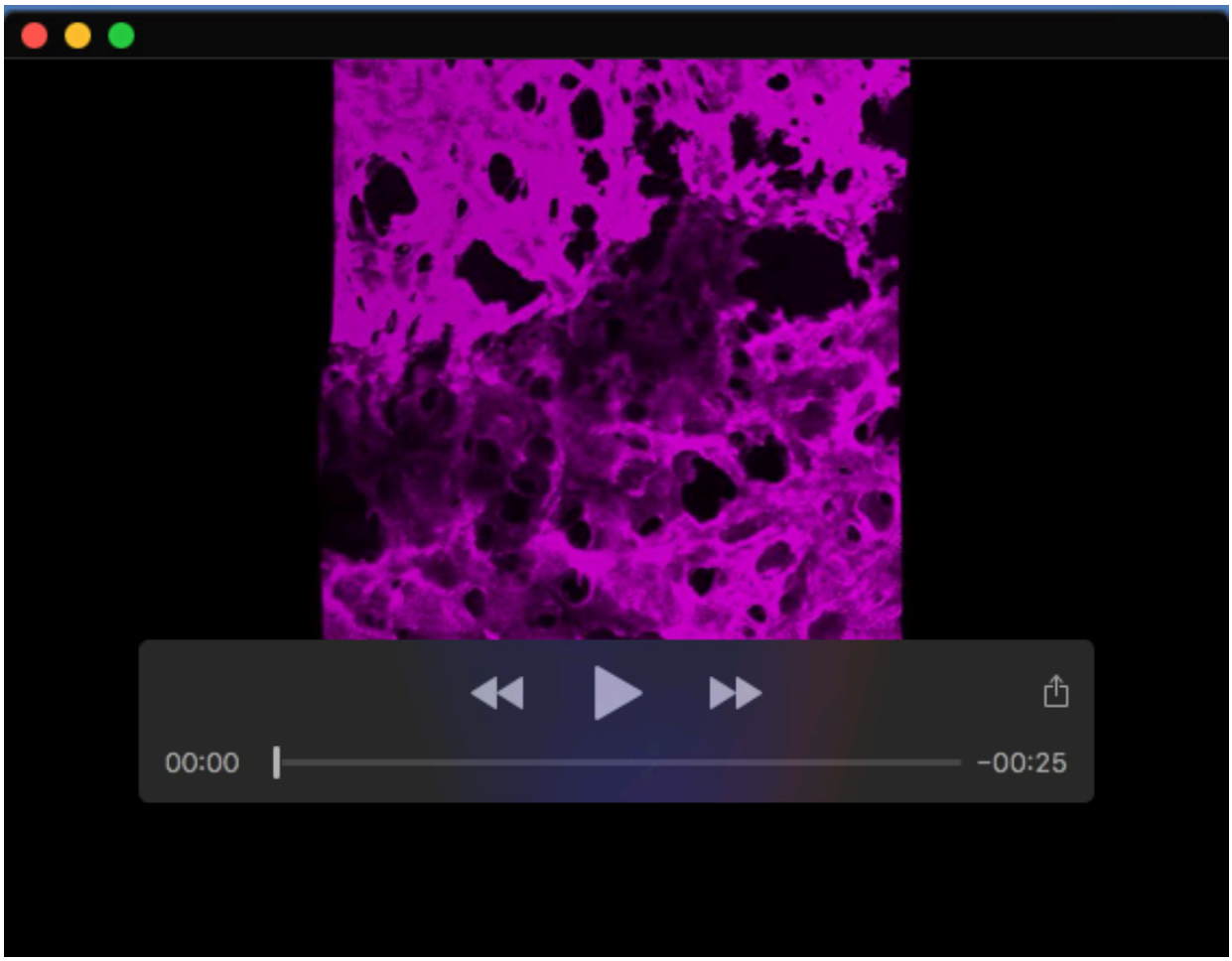

Movie 2. Projection of fused region of coronal suture from a Tcf12$^{-/-}$ mouse. 3D Confocal projection of an Alizarin Red-stained Tcf12$^{-/-}$ skull at the coronal suture. The frontal bone (bottom) and parietal bone (top) is fused together by calcified bone.

Development • Supplementary information